

Deep Learning the Forecast of Galactic Cosmic-Rays Spectra

Yi-Lun Du,^{1,*} Xiaojian Song,¹ and Xi Luo¹

¹*Shandong Institute of Advanced Technology, Jinan 250100, China*

(Dated: October 29, 2024)

We present a novel deep learning framework using Long Short-Term Memory (LSTM) networks to predict the spectra of galactic cosmic rays by leveraging historical solar activity data, addressing the limitations of traditional transport models. By incorporating multiple solar parameters, such as the heliospheric magnetic field, solar wind speed, and sunspot numbers, our model achieves accurate short-term and long-term predictions of cosmic-ray flux. The inclusion of historical cosmic-ray data enhances prediction accuracy, making the model highly effective for space weather forecasting. Moreover, it provides reliable one-day-ahead predictions of full spectra of cosmic rays for different species. Our approach surpasses traditional physics-based methods, providing a scalable, data-driven solution for reliable daily and long-term forecasts. This work paves the way for advanced models that can integrate broader observational data, with significant implications for space weather monitoring and mission planning.

I. INTRODUCTION

Cosmic rays, which are high-energy particles originating from beyond our solar system, can cause significant damage to both human health and electronic devices [1–4]. These particles, when interacting with the Earth’s atmosphere, can produce secondary particles that pose radiation risks to astronauts, aviation crews, and high-altitude populations. Moreover, cosmic rays cause ionization, which can lead to single-event upsets in electronic devices, affecting the reliability of satellite operations and ground-based electronics. Given these concerns, accurate forecasting of cosmic ray intensities is crucial for various sectors, including aerospace, telecommunications, and defense.

As galactic cosmic rays (GCRs) propagate through the heliosphere, they interact with the solar wind and the frozen-in interplanetary magnetic field. Consequently, the flux of GCRs observed near Earth is modulated by solar activity [5–21]. Solar activity, which includes various events, such as solar flares, coronal mass ejections, coronal holes, etc., can significantly alter the interplanetary environment and, consequently, the propagation of cosmic rays in the heliosphere. Understanding the solar modulation process is essential for predicting space weather events that can impact technological systems and human activities in space.

The Parker transport equation, developed by Dr. Eugene Parker, is a cornerstone in the theoretical framework for describing the propagation of GCRs and simulating their fluxes near Earth [5]. This model accounts for the essential physical processes governing the interaction between GCRs and the solar wind. It provides a comprehensive picture of how cosmic rays are scattered and transported through the heliosphere, ultimately reaching Earth.

However, the Parker transport model relies on a variety

of solar activity parameters that are challenging to quantify with precision. These include the near-Earth solar magnetic field, solar wind velocity, solar polarity, and the tilt angle of the heliospheric current sheet (HCS), among others. Additionally, the model requires the estimation of time-dependent parameters such as diffusion and drift coefficients, which are notoriously difficult to determine accurately. These uncertainties can significantly impede the accuracy of cosmic ray flux predictions [21].

Machine learning, especially deep learning, has been increasingly applied across various fields of physics and astrophysics [22–33]. In solar activity [34–38] and cosmic ray [39–50] research, machine learning has led to significant advancements in modeling and forecasting. These approaches offer new avenues for understanding the cosmic ray behavior and exploring the connection between solar activity and cosmic ray fluxes [51, 52].

In this work, we aim to address the challenges of forecasting the galactic cosmic-ray spectra near earth by employing deep learning techniques to establish a direct link between solar activity and the near-Earth GCRs spectra measured by Alpha Magnetic Spectrometer (AMS), primarily hydrogen and helium nuclei, which account for 99% in GCRs [53, 54]. By utilizing neural networks, we can automatically discover long-term, hidden correlations within historical data, thereby enhancing the predictive capabilities of our models. This approach bypasses the need for a detailed understanding of the complex transport processes, focusing instead on the empirical relationships between solar activity and cosmic ray flux.

Our methodology involves training a neural network on a dataset that integrates a broad range of solar activity parameters and historical cosmic ray flux measurements. This dataset, while limited to the AMS data range, is curated to cover a broad spectrum of solar activity variations and their potential impacts on cosmic ray flux. Key inputs, such as sunspot number (SSN)—a known indicator of solar activity correlated with cosmic ray flux modulations [55–60]—and additional cosmic ray flux data, are incorporated to help the model better capture the

* yilun.du@iat.cn

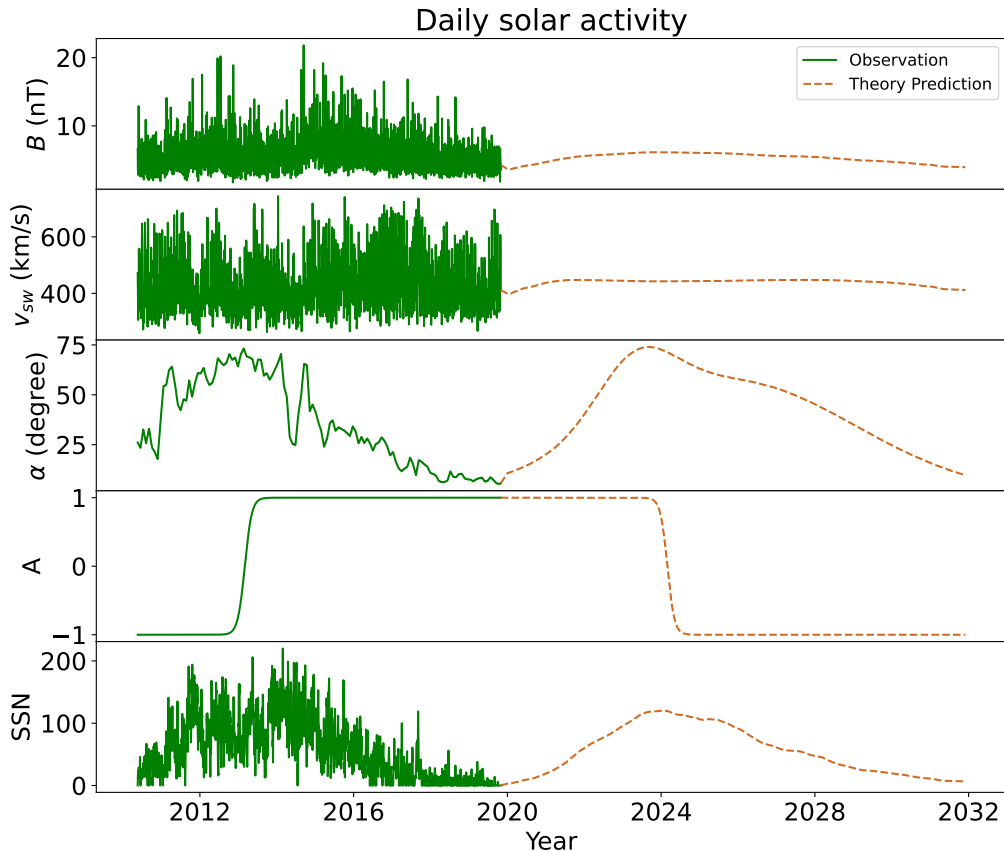


FIG. 1. Daily solar activity observed from 2011 to 2019 and predicted from 2019 to 2031 are shown as inputs to the LSTM neural network, plotted over time. The parameters displayed include the heliospheric magnetic field (HMF) (B), solar wind speed (v_{sw}) near Earth, heliospheric current sheet (HCS) tilt angle (α), solar polarity (A), and sunspot numbers (SSN).

nuances of solar activity and its effects on cosmic rays.

This approach has the potential to significantly improve cosmic ray flux prediction capabilities, contributing to a more accurate and reliable forecasting tool for mitigating the effects of space weather on critical applications in aerospace, satellite operations, and telecommunications.

The remainder of this paper is organized as follows: In Sec. II, we introduce the LSTM neural network architecture and describe the dataset preparation process. Sec. III presents the training process and prediction results under various configurations. Finally, Sec. IV provides a summary and discussion of the main findings of this work.

II. LSTM NEURAL NETWORK AND DATA PREPARATION

In this study, we utilize Long Short-Term Memory (LSTM) networks [61], a specialized form of recurrent neural network (RNN) well-suited for handling sequential data [62–64]. LSTM networks are particularly adept at addressing the vanishing gradient problem [65], a com-

mon issue in traditional RNNs that hinders the learning of long-term dependencies. The LSTM architecture, which incorporates memory cells and a gating mechanism comprising input, output, and forget gates, enables the network to selectively retain or discard information over extended periods. This selective memory capability is crucial for modeling the complex temporal dynamics of cosmic-ray fluxes, which are influenced by variable patterns in solar activity.

Our LSTM approach employs a sliding window technique to analyze local temporal variations within the one-dimensional time series of solar activity data. This method allows us to estimate both current and future cosmic-ray fluxes. Specifically, we apply a 365-day sliding window, shifted by one day, to capture the necessary temporal context for each prediction step.

The LSTM model is configured with a hidden layer comprising 64 neurons when predicting cosmic-ray flux within a single rigidity bin, and 128 neurons when predicting either the entire cosmic-ray spectrum or fluxes of different cosmic-ray species. To prevent overfitting, we incorporate dropout and recurrent dropout rates of 0.05 or 0.40 depending on whether the historical data of cosmic-rays fluxes are included as input [66, 67]. Each

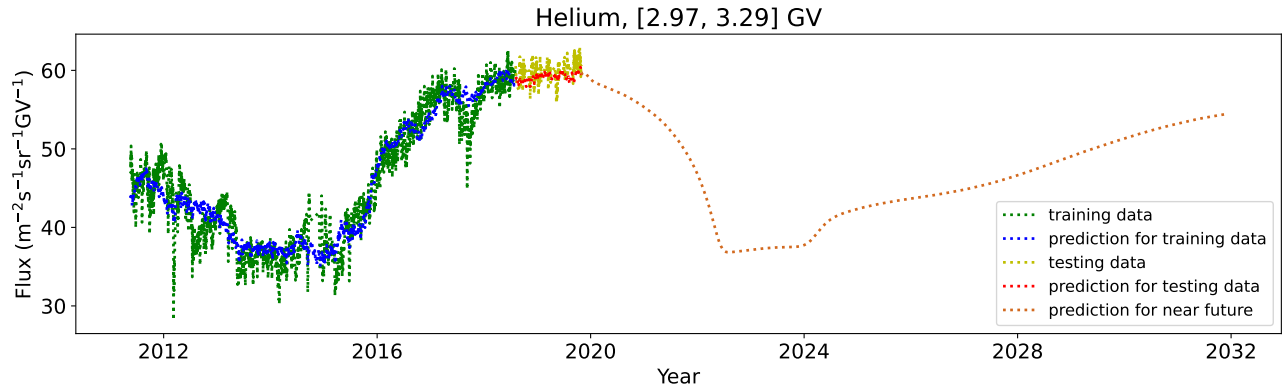


FIG. 2. Training, testing, and prediction results of Helium flux at [2.97, 3.29] GV one day ahead with four solar parameters of the past year as input. The green (yellow) dashed curve depicts the training (testing) data from AMS measurements while the blue (red) dashed curve depicts the prediction of the LSTM neural network for the training (testing) data. The chocolate dashed curve depicts the prediction of the LSTM neural network for the near future.

neuron within the hidden layer functions as a memory cell, processing incoming data, retaining pertinent information, and propagating it to subsequent time steps, thereby enhancing the network's ability to identify complex patterns.

We set the learning rate of our model to 0.0001 and conduct training for over 1000 epochs to ensure gradual convergence towards the optimal parameter space. This training process employs the Adamax gradient descent algorithm [68], which is well-suited for handling sparse gradients encountered in LSTM networks. The Huber loss function [69], which blends the properties of mean squared error and mean absolute error, is used to guide the model's accuracy, providing a robust measure of prediction performance across various discrepancies between predicted and actual values.

Our model ingests a comprehensive set of solar activity data spanning the past year, including measurements of the heliospheric magnetic field (HMF) and solar wind speed near Earth [70], HCS tilt angle [71], and solar polarity (A) [72], along with sunspot numbers (SSN) [73]. As depicted in Fig. 1, we present daily measurements of these solar activities from May 20, 2010, to October 29, 2019, along with predictions extending to December 1, 2031 from the Similar Cycle method [74–77]. To achieve daily data resolution, we apply linear interpolation to the raw data, including both the observed HCS tilt angle and predicted solar activity. Additionally, we smooth the sign of the solar polarity (A) using a Sigmoid function applied in the reverse interval to ensure smooth predictions. Before training, we normalize each solar parameter to the range [0,1] using the min-max scaling, and we set the batch size to 64 to optimize the learning process.

III. TRAINING AND PREDICTION RESULTS

In this study, we explore five different input-output setups for training our LSTM neural network model, each designed to examine the impact of various solar parameters and cosmic-ray fluxes on prediction accuracy. These setups vary in terms of the historical data used, the inclusion of specific solar and cosmic ray indicators, and the prediction goals, e.g., flux of specific elements or the entire spectrum. The following subsections detail the specific configurations and results for each setup.

A. One-Day-Ahead Prediction of Helium Flux

1. Using four solar parameters of the past year

We begin by using the same solar activity inputs as those used in the Parker transport model to train our LSTM neural network. These inputs include the observed HMF and solar wind speed near Earth, HCS tilt angle, and solar polarity (A) over a one-year period. Our primary goal is to predict the Helium flux in the rigidity range of [2.97, 3.29] GV one day in advance. The one-year input data period is selected for its influence on solar modulation of cosmic rays, capturing both short-term variations and broader trends.

For this study, we use 3085 days of Helium flux data measured by the AMS between May 20, 2011, and October 29, 2019 [78]. Of this data, the first 2,635 days, representing 85% of the total, are used for training the model, while the remaining 450 days are reserved for testing. The results of the training, testing, and prediction are presented in Fig. 2. The green dashed curve represents the training data, while the yellow dashed curve shows the testing data. The blue dashed curve corresponds to the LSTM model's predictions for the training data, and the red dashed curve shows the model's predictions for

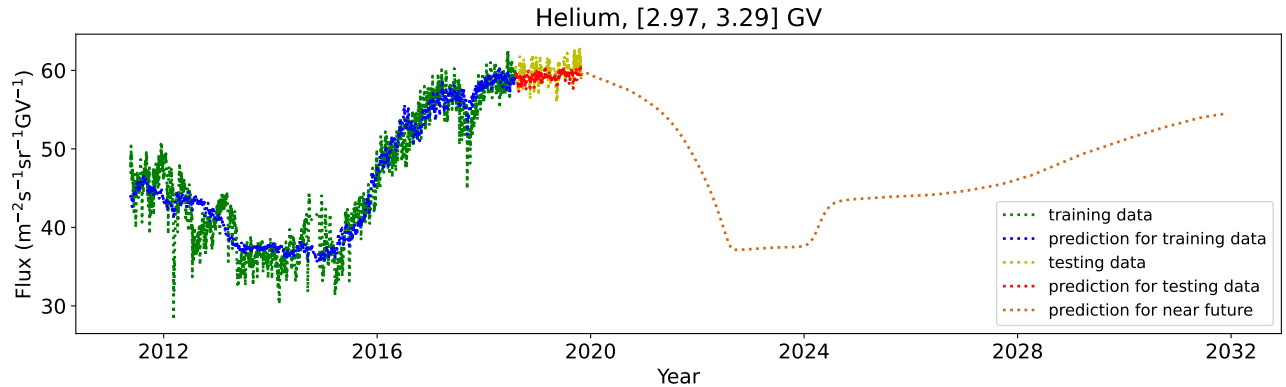


FIG. 3. Training, testing, and prediction results of Helium flux at [2.97, 3.29] GV one day ahead with five solar parameters of the past year as input. The green (yellow) dashed curve depicts the training (testing) data from AMS measurements while the blue (red) dashed curve depicts the prediction of the LSTM neural network for the training (testing) data. The chocolate dashed curve depicts the prediction of the LSTM neural network for the near future.

the testing data.

By the end of the training process, the LSTM network achieved a mean relative error of 4.65% on the training data and 1.69% on the testing data, attributed to the lower variability in the testing set. No overfitting was detected, confirming the model's robustness. Although this setup does not capture some finer structures within the training data curve, it establishes a solid baseline for subsequent discussions. We also extended the prediction into the near future, covering solar cycle 25, as shown by the chocolate dashed curve.

2. Using five solar parameters of the past year

To leverage the flexibility of neural networks, we incorporated sunspot numbers as an additional input to further enhance the prediction performance. Using the same setup as before, we achieved a mean relative error of 4.62% for the training data and 1.61% for the testing data. This improvement demonstrates that the inclusion of sunspot numbers refines the model's accuracy. We also extended the prediction into the near future, as indicated by the chocolate dashed curve in Fig. 3. The predicted trend aligns well with the results shown in Fig. 2, confirming the model's robustness and the consistency of its predictions with solar activity patterns.

In this analysis, we assess feature importance by measuring the increase in the LSTM model's mean relative error when the values of individual solar parameters are randomly shuffled. This method, known as permutation feature importance, quantifies the unique contribution of each solar parameter to the model's performance. Based on the more diverse training data, the solar parameters' importance, ranked in ascending order, is as follows: heliospheric magnetic field (HMF) near Earth (B), solar wind speed (v_{sw}) near Earth, sunspot numbers (SSN), solar polarity (A), and heliospheric current sheet (HCS)

tilt angle (α) as shown in Tab. I.

Shuffled Solar Parameters	Training Data Error	Testing Data Error
None	4.62%	1.61%
B	4.85%	1.81%
v_{sw}	5.17%	1.71%
SSN	5.44%	8.46%
A	7.05%	2.94%
α	8.97%	10.78%
All	22.4%	23.2%

TABLE I. Mean relative error with different solar parameters shuffled as input to LSTM, including cases where none, one, or all inputs are randomized.

3. Using solar parameters and Helium flux of the past year

To further enhance the prediction performance, we incorporated the past one-year flux of Helium as an additional input, a common and effective practice in time series forecasting [79]. For the initial year, when Helium flux data was unavailable, we assigned values of zero to maintain consistent data size. To mitigate error accumulation during training, we increased both the dropout and recurrent dropout rates to 0.40 in the LSTM neural network, effectively discarding 40% of the input and neuron connections at each training iteration.

We initially focused on predicting the Helium flux within the [2.97, 3.29] GV rigidity range, with training, testing, and prediction results displayed in Fig. 4. Under this configuration, the model achieved a mean relative error of 3.34% on the training data and 1.33% on the testing data, allowing for a more precise reproduction of the fine structure in the training data curve. These results represent a notable improvement in prediction accuracy over previous models, highlighting the effectiveness of in-

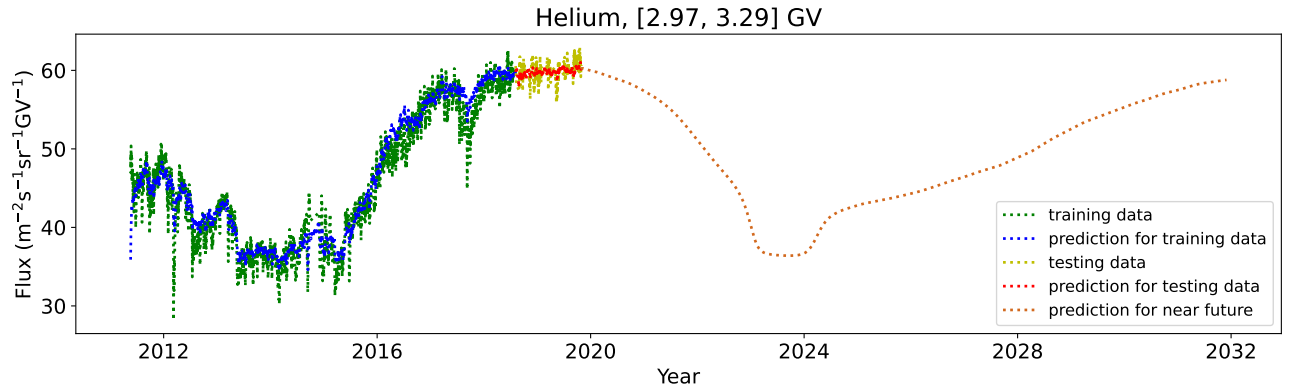


FIG. 4. Training, testing, and prediction results of Helium flux at [2.97, 3.29] GV one day ahead with five solar parameters and Helium flux at [2.97, 3.29] GV of the past year as input. The green (yellow) dashed curve depicts the training (testing) data from AMS measurements while the blue (red) dashed curve depicts the prediction of the LSTM neural network for the training (testing) data. The chocolate dashed curve depicts the prediction of the LSTM neural network for the near future.

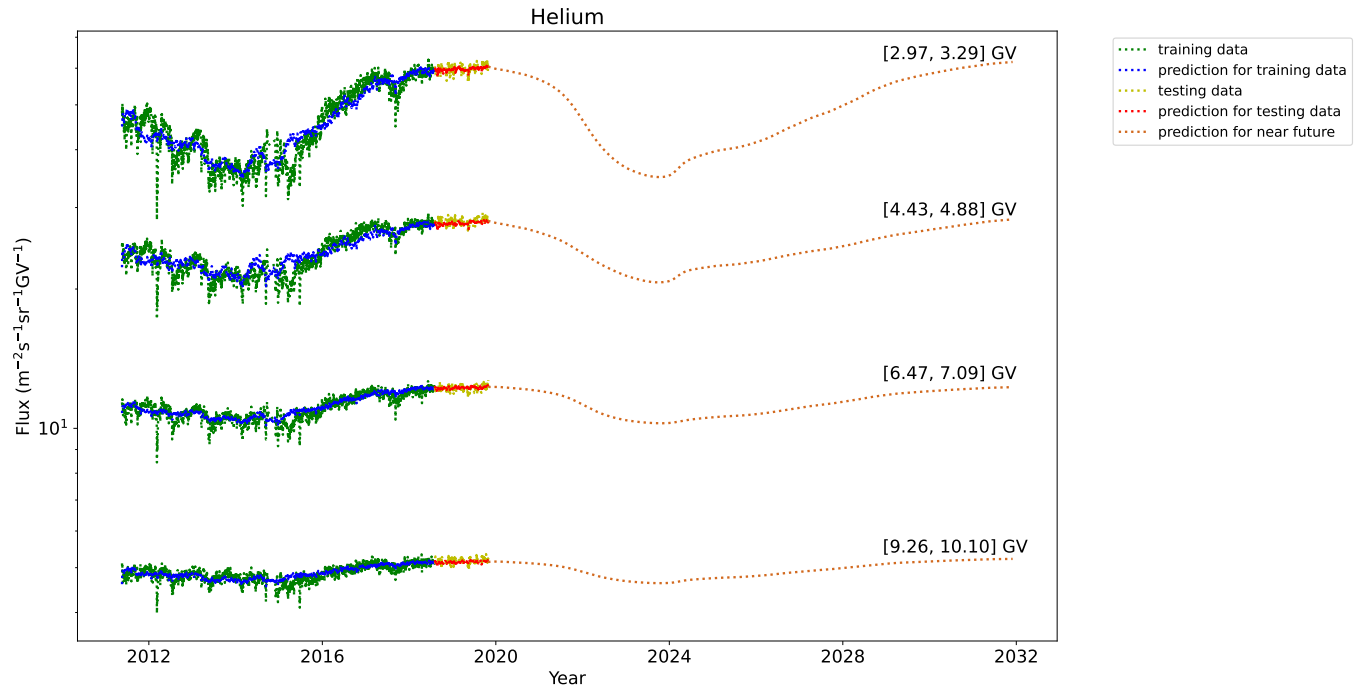


FIG. 5. Training, testing, and prediction results of Helium spectra one day ahead with five solar parameters and Helium spectra of the past year as input. The green (yellow) dashed curve depicts the training (testing) data from AMS measurements while the blue (red) dashed curve depicts the prediction of the LSTM neural network for the training (testing) data. The chocolate dashed curve depicts the prediction of the LSTM neural network for the near future.

corporating historical flux data and increasing dropout rates. Notably, in the latter phase of the near-future prediction, the model showcases a more pronounced upward trend.

B. One-Day-Ahead Prediction of Helium Spectrum

As demonstrated above, we initially focused on predicting the flux of Helium in a specific rigidity bin using

the LSTM neural network. However, it is also possible to extend this approach to predict the entire Helium spectrum using a similar LSTM network where we increase the number of neurons in the hidden layer from 64 to 128 to accommodate the increased complexity of this task. We incorporate the past one-year spectra of Helium as an additional input. The training, testing, and prediction results for four selected rigidity bins are presented in Fig. 5, indicating that the model successfully predicts the entire spectrum. For the [2.97, 3.29] GV rigidity bin,

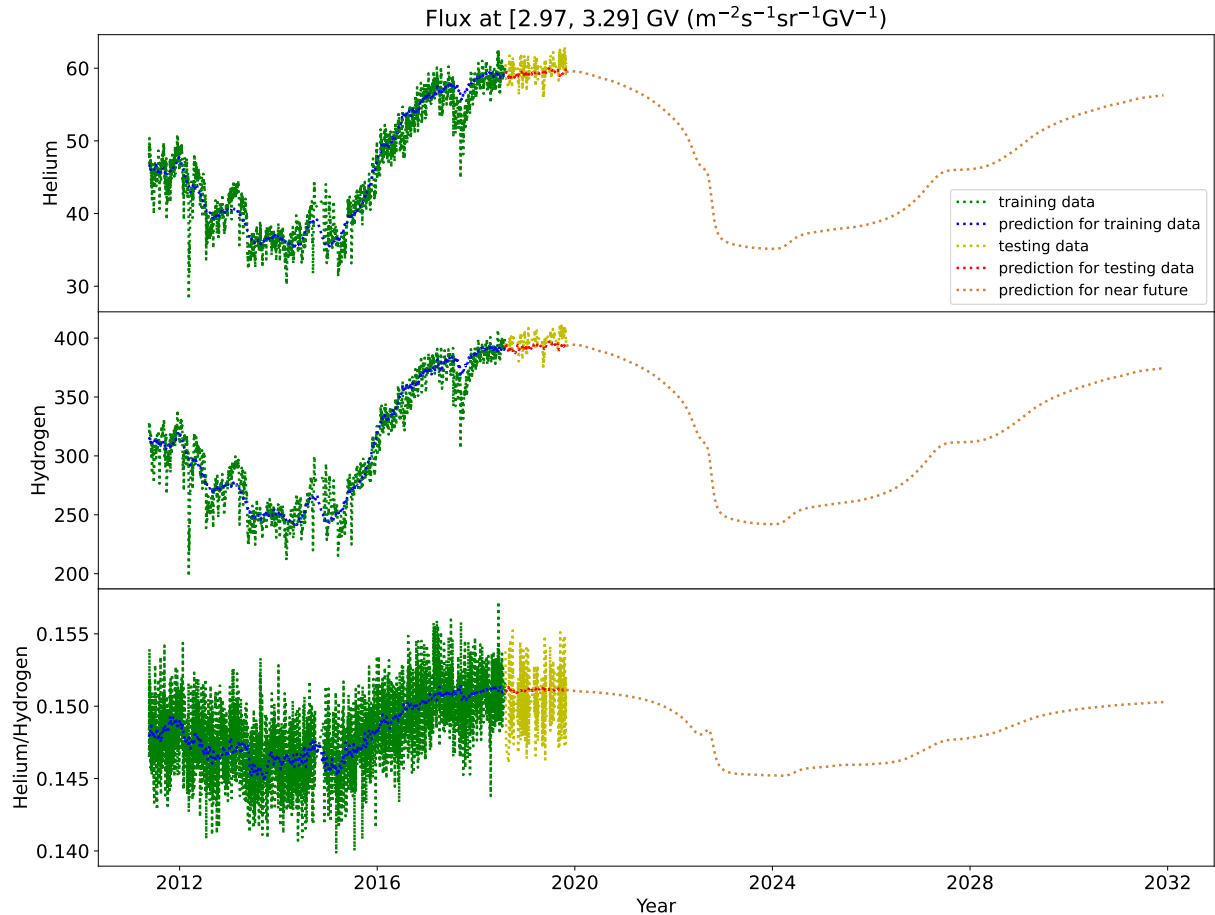


FIG. 6. Training, testing, and prediction results of Helium and Hydrogen flux as well as their ratio at [2.97, 3.29] GV one day ahead with five solar parameters of the past year as input. The green (yellow) dashed curve depicts the training (testing) data from AMS measurements while the blue (red) dashed curve depicts the prediction of the LSTM neural network for the training (testing) data. The chocolate dashed curve depicts the prediction of the LSTM neural network for the near future.

the model achieved a mean relative error of 5.27% for the training data and 1.29% for the testing data. This accuracy for the specific bin is lower than that of the earlier single-bin prediction, reflecting the trade-off in precision when expanding the model to encompass the entire spectral range. Additionally, we note that the mean relative error tends to decrease as rigidity increases.

C. One-Day-Ahead Prediction of Cosmic Ray Fluxes Across Different Species

This framework is highly generalizable for predicting the fluxes or the full spectra of various cosmic ray elements. For instance, we retrained the LSTM neural network from scratch using five solar parameters of the past year to predict the fluxes of both Hydrogen and Helium in the [2.97, 3.29] GV range simultaneously. The model achieved a mean relative error of 3.79% for the training data and 1.64% for the testing data for Helium, and 3.39% and 1.64% for Hydrogen, respectively. The

training, testing, and prediction results for the fluxes of Helium, Hydrogen, and their ratio are presented in Fig. 6, further demonstrating the model's robustness across different elements. Notably, the helium-to-hydrogen flux ratio follows a trend similar to that of the hydrogen flux itself.

D. Helium Flux Prediction Integrating Multiple Model Setups

For predicting Helium flux in the [2.97, 3.29] GV rigidity range in the near future, we observed discrepancies across the results from these different model setups. To address this, we averaged the results from each setup and quantified uncertainty using their root mean square deviation. The final prediction, along with the associated uncertainty, is illustrated as the chocolate-colored band in Fig. 7.

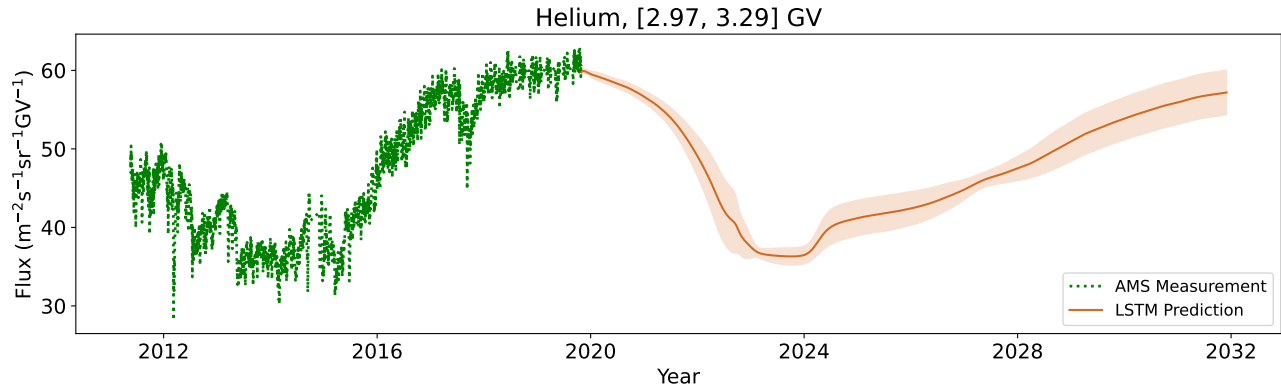


FIG. 7. The green dashed curve depicts the AMS measurements for Helium flux at [2.97, 3.29] GV, while the chocolate-colored band shows the LSTM neural network's near-future prediction, averaged across different model setups.

IV. CONCLUSIONS

In this work, we establish, for the first time, a robust correspondence between historical solar activity and cosmic ray flux near Earth using Long Short-Term Memory (LSTM) networks, a deep learning technique. We also apply permutation feature importance to evaluate each solar parameter's unique contribution to the model's performance, enhancing our understanding of parameter influence. This framework allows the inclusion of diverse solar activity data, such as sunspot numbers, and opens the door to incorporating a broader range of observational data for improved predictive performance. Unlike traditional transport models, which are limited in integrating varied inputs, our deep learning approach demonstrates greater flexibility and adaptability with diverse datasets.

Including historical cosmic ray flux data is especially effective in improving the accuracy of short-term, one-day-ahead predictions. This capability is valuable for space weather forecasting, where precise and timely predictions are essential to mitigate cosmic ray effects on human health and technology. For long-term predictions, we mitigate error accumulation by applying a higher dropout rate during LSTM training, which helps maintain stability in extended forecasting.

By exploring various modeling schemes, our frame-

work demonstrates the ability to reliably predict cosmic ray spectra across species and timescales, from daily to decadal forecasts. These results showcase the potential of machine learning to surpass traditional physics-based models in certain aspects, offering a scalable, data-driven solution. Our approach not only advances cosmic ray forecasting accuracy but also lays a foundation for future improvements, such as incorporating additional solar and cosmic ray data as they become available.

In summary, this study demonstrates the feasibility and advantages of applying deep learning to cosmic ray flux prediction, paving the way for more advanced models to support space weather monitoring, technological protection, and future space mission planning.

ACKNOWLEDGMENTS

We appreciate the insightful discussions with Weiwei Xu, Ran Huo, Kai Zhou, Zhaoming Wang, Yao Chen, and Sisi Wang. This work is supported by the Taisan Scholars Program of Shandong Province under Grant No. tsqnz20221162 (Y. D.) and Grant No. 202103143 (X. L.), the Shandong Excellent Young Scientists Fund Program (Overseas) under Grant No. 2023HWYQ-106 (Y. D.), the NSFC under Grant No. U2106201 (X. L.) and Grant No. 42404172 (X. S.), and the Natural Science Foundation of Shandong Province under Grant No. ZR2022QD033 (X. S.).

[1] F. A. Cucinotta, M. Alp, F. M. Sulzman, and M. Wang, *Life Sci. Space Res.* **2**, 54 (2014).

[2] L. C. Simonsen, T. C. Slaba, P. Guida, and A. Rusek, *PLOS Biol.* **18**, e3000669 (2020).

[3] W. C. de Wet, T. C. Slaba, F. Rahmanifard, J. K. Wilson, A. P. Jordan, L. W. Townsend, N. A. Schwadron, and H. E. Spence, *Life Sci. Space Res.* **26**, 149 (2020).

[4] X. Chen, S. Xu, X. Song, R. Huo, and X. Luo, *Space Weather* **21**, e2022SW003285 (2023).

[5] E. N. Parker, *Planet. Space Sci.* **13**, 9 (1965).

[6] J. Quenby, *Space Sci. Rev.* **37**, 201 (1984).

[7] J. Simpson, *Space Sci. Rev.* **83**, 169 (1998).

[8] X. Luo, M. Zhang, H. K. Rassoul, and N. V. Pogorelov, *ApJ* **730**, 13 (2011).

[9] J. Kóta, *Space Sci. Rev.* **176**, 391 (2013).

[10] X. Luo, M. Zhang, H. K. Rassoul, N. V. Pogorelov, and

J. Heerikhuisen, ApJ **764**, 85 (2013).

[11] M. S. Potgieter, Living Rev. Sol. Phys. **10**, 3 (2013).

[12] M. Potgieter, Braz. J. Phys. **44**, 581 (2014).

[13] P. O'Neill, S. Golge, and T. Slaba, *Badhwar-O'Neill 2014 galactic cosmic ray flux model description*, Tech. Rep. (2015).

[14] E. E. Vos and M. S. Potgieter, ApJ **815**, 119 (2015).

[15] E. Vos and M. Potgieter, Sol. Phys. **291**, 2181 (2016).

[16] X. Luo, M. S. Potgieter, M. Zhang, and X. Feng, ApJ **839**, 53 (2017).

[17] M. Potgieter, Adv. Space Res. **60**, 848 (2017).

[18] Z.-N. Shen, G. Qin, P. Zuo, and F. Wei, ApJ **887**, 132 (2019).

[19] X. Luo, M. Zhang, X. Feng, M. S. Potgieter, F. Shen, and G. Bazilevskaya, ApJ **899**, 90 (2020).

[20] M. Aguilar, L. A. Cavasonza, G. Ambrosi, L. Arruda, N. Attig, F. Barao, L. Barrin, A. Bartoloni, S. Bağışmezdu Pree, R. Battiston, *et al.*, Phys. Rev. Lett. **127**, 271102 (2021).

[21] X. Song, X. Luo, M. S. Potgieter, X. Liu, and Z. Geng, ApJS **257**, 48 (2021).

[22] J. Carrasquilla and R. G. Melko, Nat. Phys. (2017).

[23] K. Ch'ng, J. Carrasquilla, R. G. Melko, and E. Khatami, Phys. Rev. X **7**, 031038 (2017).

[24] L.-G. Pang, K. Zhou, N. Su, H. Petersen, H. Stöcker, and X.-N. Wang, Nature Commun. **9**, 210 (2018).

[25] G. Carleo, I. Cirac, K. Cranmer, L. Daudet, M. Schuld, N. Tishby, L. Vogt-Maranto, and L. Zdeborová, Rev. Mod. Phys. **91**, 045002 (2019).

[26] Y.-L. Du, K. Zhou, J. Steinheimer, L.-G. Pang, A. Mottoronenko, H.-S. Zong, X.-N. Wang, and H. Stöcker, Eur. Phys. J. C **80**, 1 (2020).

[27] Y.-L. Du, D. Pablos, and K. Tywoniuk, JHEP **21**, 206 (2020).

[28] Y.-L. Du, D. Pablos, and K. Tywoniuk, Phys. Rev. Lett. **128**, 012301 (2022).

[29] K. Zhou, G. Endrődi, L.-G. Pang, and H. Stöcker, Phys. Rev. **D100**, 011501 (2019).

[30] S. Shi, K. Zhou, J. Zhao, S. Mukherjee, and P. Zhuang, Phys. Rev. D **105**, 014017 (2022).

[31] A. Boehlein, M. Diefenthaler, N. Sato, M. Schram, V. Ziegler, C. Fanelli, M. Hjorth-Jensen, T. Horn, M. P. Kuchera, D. Lee, *et al.*, Rev. Mod. Phys. **94**, 031003 (2022).

[32] J. VanderPlas, A. J. Connolly, Ž. Ivezić, and A. Gray, in *2012 conference on intelligent data understanding* (IEEE, 2012) pp. 47–54.

[33] D. George and E. Huerta, Phys. Rev. D **97**, 044039 (2018).

[34] R. Qahwaji and T. Colak, Sol. Phys. **241**, 195 (2007).

[35] T. Colak and R. Qahwaji, Space Weather **7** (2009).

[36] C. Voyant, G. Notton, S. Kalogirou, M.-L. Nivet, C. Paoli, F. Motte, and A. Fouilloy, Renew. Energy **105**, 569 (2017).

[37] S. Malinović-Milićević, M. M. Radovanović, S. D. Radenković, Y. Vyklyuk, B. Milovanović, A. Milanović Pešić, M. Milenović, V. Popović, M. Petrović, P. Sydor, *et al.*, Mathematics **11**, 795 (2023).

[38] S. Kasapis, I. N. Kitiashvili, A. G. Kosovichev, J. T. Stefan, and B. Apte, arXiv preprint arXiv:2402.08890 (2024).

[39] P. Paschalidis, C. Sarlanis, and H. Mavromichalaki, Sol. Phys. **282**, 303 (2013).

[40] M. Erdmann, J. Glombitza, and D. Walz, Astropart. Phys. **97**, 46 (2018).

[41] S.-J. Lin, X.-J. Bi, and P.-F. Yin, Phys. Rev. D **100**, 103014 (2019).

[42] P. Schichtel, M. Spannowsky, and P. Waite, EPL **127**, 61002 (2019).

[43] K. Zhang and J. S. Bloom, ApJ **889**, 24 (2020).

[44] R. Acciari, C. Adams, C. Andreopoulos, J. Asaadi, M. Babicz, C. Backhouse, W. Badgett, L. Bagby, D. Barker, V. Basque, *et al.*, Front. Artif. Intell. **4**, 649917 (2021).

[45] O. Mandrikova and B. Mandrikova, Symmetry **14**, 744 (2022).

[46] T. Bister, M. Erdmann, U. Köthe, and J. Schulte, Eur. Phys. J. C **82**, 1 (2022).

[47] Y.-L. S. Tsai, Y.-L. Chung, Q. Yuan, and K. Cheung, J. Cosmol. Astropart. Phys. **2022**, 044 (2022).

[48] A. Alvarado, T. Capistrán, I. Torres, J. Sacahuí, and R. Alfaro, arXiv:2310.06938 (2023).

[49] T. Hachaj, L. Bibrzycki, and M. Piekarczyk, IEEE Access **11**, 7410 (2023).

[50] M. Y. Kuznetsov, N. Petrov, I. Plokikh, and V. Sotnikov, J. Cosmol. Astropart. Phys. **2024**, 125 (2024).

[51] B. Belen, U. Leloglu, and M. Demirköz, Adv. Space Res. (2024).

[52] A. Polatoglu, IJCESEN **10** (2024).

[53] J. Simpson, Annu. Rev. Nucl. Sci. **33** (1983).

[54] T. K. Gaisser, Comments Nucl. Part. Phys. **11**, 25 (1982).

[55] S. E. Forbush, J. Geophys. Res. **59**, 525 (1954).

[56] S. E. Forbush, J. Geophys. Res. **63**, 651 (1958).

[57] E. Cliver and A. Ling, ApJ **556**, 432 (2001).

[58] A. Mishra, M. Gupta, and V. Mishra, Sol. Phys. **239**, 475 (2006).

[59] E. Ross and W. J. Chaplin, Sol. Phys. **294**, 1 (2019).

[60] S. A. Koldobskiy, R. Kähkönen, B. Hofer, N. A. Krivova, G. A. Kovaltsov, and I. G. Usoskin, Sol. Phys. **297**, 38 (2022).

[61] S. Hochreiter, Neural Comput. (1997).

[62] Y. Hua, Z. Zhao, R. Li, X. Chen, Z. Liu, and H. Zhang, IEEE Commun. Mag. **57**, 114 (2019).

[63] A. Tealab, FCIJ **3**, 334 (2018).

[64] H. Sak, A. Senior, and F. Beauvais, in *Fifteenth annual conference of the international speech communication association* (2014).

[65] S. Basodi, C. Ji, H. Zhang, and Y. Pan, Big Data Min. Anal. **3**, 196 (2020).

[66] N. Srivastava, G. E. Hinton, A. Krizhevsky, I. Sutskever, and R. Salakhutdinov, J. Mach. Learn. Res. **15**, 1929 (2014).

[67] S. Semeniuta, A. Severyn, and E. Barth, arXiv preprint arXiv:1603.05118 (2016).

[68] D. P. Kingma and J. Ba, arXiv:1412.6980 (2014).

[69] P. J. Huber, Ann. Math. Stat. **35**, 73 (1964).

[70] spdf.gsfc.nasa.gov.

[71] wso.stanford.edu/Tilts.

[72] wso.stanford.edu/Polar.

[73] sdc.be.

[74] J. MIAO, J. WANG, S. LIU, and J. GONG, CJSS **27**, 448 (2007).

[75] J. Wang, J. Miao, S. Liu, J. Gong, and Z. Cuilian, Sci. China- Phys. Mech. Astron. **38**, 1097 (2008).

[76] J. Miao, J. Gong, Z. Li, and R. Tingling, Sci. China- Phys. Mech. Astron. **45**, 099601 (2015).

[77] J. Miao, X. Wang, T.-L. Ren, and Z.-T. Li, Res. Astron.

Astrophys. **20**, 004 (2020).

[78] M. Aguilar, L. A. Cavasonza, G. Ambrosi, L. Arruda, N. Attig, F. Barao, L. Barrin, A. Bartoloni, S. Başegmezdu Pree, R. Battiston, *et al.*, Phys. Rev. Lett. **128**, 231102 (2022).

[79] R. Lam, A. Sanchez-Gonzalez, M. Willson, P. Wirnsberger, M. Fortunato, F. Alet, S. Ravuri, T. Ewalds, Z. Eaton-Rosen, W. Hu, *et al.*, Science **382**, 1416 (2023).